Title: Iron-Catalyzed Aza-Annulative π-Extension with Alkynes via C–H Activation using an Oxidative Auxiliary

Authors: Yan Zhang[1], Shota Fukuma[1], Rui Shang[1],* and Eiichi Nakamura[1]*

Affiliations:

[1] Department of Chemistry, School of Science, The University of Tokyo, 7-3-1 Hongo, Bunkyo-ku, Tokyo 113-0033, Japan.

* e-mail: rui@chem.s.u-tokyo.ac.jp (R.S.); nakamura@chem.s.u-tokyo.ac.jp (E.N.)

Abstract: Aza-annulative π-extension (**AAPE**) reactions offer a potent pathway to create novel donor-acceptor conjugated materials by integrating an imine moiety into the conjugated system, serving as an electron-accepting unit. However, the affinity of late-transition metals for conjugated π-systems, coupled with their elevated cost, has posed significant challenges, restricting efficient **AAPE** reactions on straightforward C–H substrates for developing conjugated new materials. In this study, we unveil an iron-catalyzed C–H activation methodology, facilitating **AAPE** with diverse internal alkynes and employing oxime ether as both a self-oxidizing auxiliary and nitrogen source, derived seamlessly from accessible carbonyl compounds. The **AAPE** reaction was enabled by using trisphosphine as a ligand, and isobutyl aluminum(III) catecholate as a base. By using the reaction, we discovered an aza-oxa[5]helicene from dixanthone as a potential circularly polarized luminescence material and two narrow-band-emissive molecules from easily accessible pentacene-6,13-dione and quinacridone, which emit blue and yellow light with high color purity and high fluorescence quantum yield. These findings emphasize the potential of iron-catalyzed C–H activation in expanding the range of donor-acceptor-type conjugated materials for organic electronics.

Main Text: The affordability and sustainability of iron[1] have spurred its adoption in the discovery and fabrication of conjugated materials, leveraging innovative iron-catalyzed transformations for accessing π-

conjugated molecules. Aza-annulative π-extension (**AAPE**) reactions are particularly appealing for their capacity to efficiently create complex fused aza-arene structures on conjugated molecules.[2] These reactions integrate imine moieties as an acceptor-units into conjugated systems (Figure 1), giving rise to donor-acceptor systems with unique material properties.[3] As depicted in Figure 1A, such an iron-catalyzed **AAPE** reaction ideally uses easily accessible carbonyl compounds, which are conveniently generated by the oxidation of aromatic hydrocarbons[4] or condensation[5], through direct C–H bond activation in the presence of a nitrogen source and an alkyne. This methodology is exemplified in its application to pentacenequinone[6] and quinacridone[7-11], precursors in the manufacture of classical organic semiconductors and pigments, enabling the cost-effective production of novel electronic materials (Figure 1B). However, challenges persist in iron-catalyzed C–H activation. Despite the development of over a decade[12], issues like the limited range of directing groups and the competition from oxidative C–H coupling with carbon nucleophiles, employed as bases for deprotonative C–H activation, remain formidable obstacles to efficient iron-catalyzed **AAPE** reactions.

In this study, we successfully surmounted these problems to develop efficient iron-catalyzed **AAPE** reactions through C–H activation. We identified oxime ether[13], easily installed via the condensation of *N*-methoxy amine with carbonyl in the presence of Lewis acids, as a multifunctional element. It serves as an effective directing group, an internal oxidant facilitating catalyst turnover, and the nitrogen source essential for azaoarene formation. An isobutyl aluminum(III) catecholate, easily generated by reacting commercially available triisobutylaluminum solution in toluene with one equivalent amount of catechol, acts as a base for deprotonative C–H activation, successfully suppressing undesired C–H coupling with the base. As depicted in Figure 1C for the hypothesized reaction mechanism, isobutyl catecholato aluminum(III) functions as a base. It facilitates the transmetallation of the alkyl group to Fe(III) and deprotonates the *ortho*-C–H bond, leading to the formation of isobutane and a ferracycle intermediate (**I**). The insertion of the alkyne into the Fe-C bond of intermediate **I** results in a seven-membered ring ferracycle (**II**). This intermediate (**II**) then undergoes reductive elimination, yielding an

N-methoxy pyridinium that acts as an oxidant, turning Fe(I) back to Fe(III). The oxophilic aluminum (III) captures the methoxy anion, preventing it from coordinating with Fe(III), which would otherwise poison the catalyst. The reaction is generally applicable for a variety of conjugated carbonyl compounds and a broad scope of alkynes including but-2-yne that produces methylated aza-arenes in high yields (*vide infra*), providing expedient access to π-extended aza-arenes to discover their utilities as electronic materials[14-16]. We anticipate the catechol effect discovered herein will be instrumental for the future development of other types of efficient iron-catalyzed C–H activation reactions.

Our effort was first to identify a suitable organometallic base for chemoselective C–H activation. In our previous works, we demonstrated the efficacy of trimethylaluminum as a base in iron-catalyzed C–H activation reactions.[17-20] The milder nucleophilicity and lower reducibility of carbon-Al bond compared with Grignard reagent and organozinc reagents accounts for the high efficacy in Fe(III)-catalyzed C–H activation. However, the undesired fast C–H alkylation after ferracycle formation constraints further development of versatile C–H functionalization reactions beyond C–H methylation. We hypothesized that reducing the nucleophilicity of the alkyl aluminum reagent by quenching two of the three alkyls on aluminum may suppress the undesired further transmetallation and hence allow the ferracycle to undergo insertion with an alkyne. We considered a relatively bulky alkyl may slow down Al-Fe transmetallation in comparison to $AlMe_3$. The hypothesis prompted us to test using catechol to quench triisobutyl aluminum, Al(*i*-Bu)$_3$, a commercially available aluminum reagent sold as a solution in toluene.

Iron-catalyzed **AAPE** reaction using 10-methylacridin-9(10*H*)-one *O*-methyl oxime (**1**) and diphenyl acetylene by using a benzofuryl trisphosphine (**TP1**)[21] as ligand and Al(*i*-Bu)$_3$/catechol provided aza-annulation product (**3**) quantitively. The combination of catechol with Al(*i*-Bu)$_3$ generating a formular of *i*-BuAl·catecholate mitigates the nucleophilicity of organoaluminium base, and suppressed undesired side reactions such as C–H alkylation. The *β*-H-elimination[22], which was known to poison the catalytic cycle of C−H activation, was also suppressed.

The detailed condition for iron-catalyzed **AAPE** reaction using 10-methylacridin-9(10*H*)-one *O*-methyl oxime (**1**) with diphenyl acetylene is shown in Figure 2 (top equation). The *O*-methyl oxime was easily synthesized from the corresponding ketone in high yield (95% for **1**). To a Schlenk tube charged with oxime ether (**1**), tolane (1.5 equiv), $Fe(acac)_3$ (10 mol %), **TP1**, and catechol (200 mol%) was added xylene followed by slow addition of a solution of Al(*i*-Bu)$_3$ in toluene at room temperature. The reaction mixture was stirred at r.t. for 5 mins to allow generation of *i*-BuAl·catecholate in-situ. Up heating at 140 °C for 24h, the reaction yielded the cyclization product quantitatively as indicated by ^{1}H-NMR analysis.

The data in Figure 2 illustrate some reaction parameters affecting the **AAPE** reaction. Iron catalyst, catechol, and Al(*i*-Bu)$_3$ are all essential for the reaction to take place (entry 1, 3, and 4). While a low yield of 25 % of **2** was observed in the absence of **TP1**. Reducing the loading of iron and ligand to 5 mol % and 6 mol % still gave **2** in 90% yield. However, only 23% of **2** could be generated using iron catalyst in 1 mol % (Figure 2, entries 5 and 6). Lower temperatures to 120 °C slowed down the reaction (entry 7). Using THF as solvent instead of xylene also produced **2** in quantitative yield (entry 8), while xylene is preferred solvent for large p-extended substrates for solubility issues. Using $AlMe_3$ instead of Al(*i*-Bu)$_3$ slightly inhibited the reaction probably due to the above-mentioned fast methyl transmetallation and side reaction. A side reaction to give *N*-methyl imine was detected indicating the nucleophilic methyl group replaces the *N*-methoxyl substituent of oxime ether (entry 9). We also assessed the amount and ratio of catechol to Al(*i*-Bu)$_3$. Excess catechol resulted in a sharp decrease of the yield to 18% yield probably due to over quenching of the alkyls (entry 10). However, reducing the catechol equivalent to Al(*i*-Bu)$_3$ did not affect much the efficiency of highly reactive substrates (entry 11). The amount of *i*-BuAl·catecholate can be reduced to 1.5 equivalent without affecting the reaction efficiency of **1**.

The influence of ligand on the reaction outcome is depicted in Figure 3A. Different from our previously observed ligand effects for iron-catalyzed C–H activation reactions[18-20], where only a certain structure of ligand was uniquely effective, this particular **AAPE** reaction exhibited a certain level of

tolerance to diverse ligand structures. The desired cyclization product **2** was obtained in 25% yield even in the absence of a **TP** ligand. We speculate that aluminum catecholate may interact with iron in this reaction system to stabilize the iron species in the catalytic cycle[23]. Besides the optimal ligand (**TP1**), **TP2** and triphos were also effective to yield **2** in 88% and 85%, respectively. Interestingly, besides tridentate phosphine ligands; bisphosphine ligands such as dppbz and dppe were also effective to give decent yields. Even tetradentate phosphine ligand (TetraP) gave **2** in 74% yield. In contrast, monodentate phosphine ligand (PPh_3) and pyridine-type ligands such as dtbpy or terpy were ineffective. The ligand dependence observed implies the coordination environment of iron in the catalytic cycle varies as ligand dissociation and association may occur[24], which will be subjected to our further mechanistic studies.

Next, we showed the effects of various phenol derivatives (Figure 3B). Although we used to consider that alkoxide and phenoxide may poison iron species by their strong coordination[25], our recently reported Fe(III)/$AlMe_3$/**DEO** (diethyl oxalate) catalytic system[19] revealed that in the presence of AI(III), enediolate does not affect the catalytic activity of iron for C–H activation. Besides catechol, using naphthalene-1,8-diol also afforded **2** quantitatively. Using phenol in 4.0 equivalents also gave a high yield, but the sterically congested 2,6-diphenylphenol and 2,6-di-tert-butyl-4-methylphenol, which are known to form bulky $(ArO)_2AlR$ reagent[26], resulted in poor reaction efficacy. The reduced efficacy caused by steric hindrance may be ascribed to suppressing effective transmetallation, preventing them as effective base. The ineffectiveness of 2-methoxyphenol might be attributed to the occupation of the coordination fourth site of Al(III) by the additional methoxyl group, impeding the transmetallation step. Surprisingly, using 2-hydroxythiophenol yielded **2** in 87%, but thiophenol in 4 equivalents gave no reactivity. We attribute this observation to variations in the affinity of 2-hydroxythiophenol and thiophenol for iron and aluminum. Pinacol used instead of catechol suppressed the reaction entirely, which might be because of the strong coordination of alkoxide towards iron.

To further corroborate the proposed role of catechol, we tried to generate *i*-BuAl·catecholate (***i*-BuAlC**) by mixing Al(*i*-Bu)$_3$ with catechol in toluene/xylene. The reaction performed using ***i*-BuAlC**

gave a quantitative yield as illustrated in Figure 4A. To understand whether the stereochemistry of oxime ether (Z and E) affects the selectivity of this **AAPE** process. An intramolecular competition experiment employing oxime ether derived from 4-(trifluoromethyl)benzophenone as 1:1 ratio of E/Z mixture was tested. As the acidity of C–H bonds affects regioselectivity of iron(III)-catalyzed deprotonative C–H activation, cyclization product **a** should be major isomer if the C–H site selectivity is not determined by Z/E ratio of oxime ether. A ratio of **a/b = 4/1** was obtained indicating that the acidity of C−H bonds but not the stereoisomerism of oxime ether determines the selectivity.

Figure 5 describes the substrate scope. The iron-catalyzed system is highly effective for π-extended oxime ether substrates. The oxime ether substrates derived from acridinone (**2** and **4**), xanthenone (**5**), thioxanthenone (**6**), and anthrone (**7**) all reacted quantitatively resulting annulation products easily purified by silica gel chromatography or recrystallization. The **AAPE** reaction also works well with spiro-conjugated carbocycles to give a new spiro-conjugated aza-arene (**8**) in 81% yield. Oxime ether derived from seven-membered-ring dibenzosuberenone yielded the desired product in 86% yield (**9**) but the five-membered-ring fluorenone failed to react (**10**), which was attributed to the difference in N=C–C bond angles for ferracycle formation. This difference in C–H activation reactivity was also observed in carbonyl directed C−H methylation[18]. An aza-pyrene framework can be easily constructed from phenalenone (**11**). **AAPE** was compatible with flavone and 7,8-benzoflavone producing unprecedented aza-arenes skeletons from these bio-active nature products for possible medicinal applications[27] (**17** and **18**). The relatively low yield of flavone is ascribed to its competitive decomposition[28]. A variety diaryl acetylenes possessing different substituents with electronic properties, including methoxyl (**13**, **21**, **22**), bromide (**14**), trifluoromethyl (**15**), and alkyls (**19** and **20**) all reacted smoothly. Besides tolane derivatives, dialkyl acetylenes are also well compatible (**12**, **23**–**26**). Notably, methylated aza-arenes can be obtained using 2-butyne in quantitative yield (**23**). Methylation has proven to be an effective strategy for enhancing not only the efficiency of compounds in medicinal chemistry[29] but also, more recently, in the field of electronic materials science[30].

For unsymmetrical alkynes, trimethyl(phenylethynyl)silane and 1-phenyl-1-hexyne were tested and high yields along with high regioselectivity were obtained (**27** and **28**). The excellent regioselectivity can be explained by the stability of Fe-C bond at the α-styrenyl position (intermediate II in Figure 1C), π-conjugation, as well as the steric effects illustrated in the inset figure. TIPS-protected phenylacetylene failed because of the large steric hindrance (**29**). Leveraging this regioselectivity, a double cyclization of **1** with 1,4-bis((trimethylsilyl)ethynyl)benzene provided a phenylene-linked conjugated structure in 61% yield as a pure regioisomer (**30**). The TMS substituents can function as a synthetic handle for further derivatization and annulation.[31] The access to two π-extended structures from chromeno[3,2-*c*]xanthene-5,8-dione[32] (**31** and **32**) was also achieved via a double cyclization**.** These molecules with an extended p-system and a donor-acceptor structure are worth exploring further to investigate their optoelectronic and charge transport properties for potential applications in electronic materials.

The double **AAPE** reaction also facilitated the construction of a helical-bischromenoisoquinoline (**Heli-BCIQ, 33**) from chromeno[3,2-*a*]xanthene-13,14-dione[32] (Figure 6A). An initial examination of the optoelectronic characteristics of **33** showed a green emission, with a photoluminescence quantum yield (PLQY) of 23.0% (See Figure S4). The structure of **Heli-BCIQ** was demonstrated by single crystal X-ray analysis, displayed as mirror-image plots for the (M) and (P) enantiomers (Figure 6B). Further investigations were intended on the properties of **Heli-BCIQ**, especially applied on devices as potential candidates for circularly polarized luminescence (CPL) materials.[33] The packing structure of **Heli-BCIQ** showed homochiral stacking along [110] direction (Figure 6c) and along [1-10] (Figure 6d), forming two-dimensional homochiral assembly. The nearby heterochiral layers form characteristic zipper-like p-stacking with a distance of 3.27 Å.

Application of this iron-catalyzed **AAPE** reaction on conjugated ketones that are easily available as either organic semiconductors or pigments to construct new conjugated skeletons for developing electronic materials are certainly attractive. We decided to test this possibility on pentacene-6,13-dione, a precursor for synthesizing pentacene[34] and also the product of pentacene oxidation[35], to provide

pentacene-π-extended aza-arene.[36-37] The five linearly fused benzene ring resulted in elevated HOMO level, making the conjugated molecule sensitive towards to chemical oxidant. The large π-conjugation also increases propensity of π-coordination toward a transition metal thus inhibiting desired reactivity of a transition metal catalyst. To our delight, reaction of oxime ether derived from pentacene-6,13-dione afforded anthra[1,2,3,4-*lmn*]benzo[*f*][2,9]phenanthroline (abbreviated as **ABPhen, 34**) as a single product quantitatively (Figure 7A). The possible regioisomer of benzo[5,6]isoquinolino[1,8-*gh*]naphtho[1,2,3-*de*]quinoline was not formed. The selectivity of the CH sites for the second cyclization could be explained by the acidity of C–H bonds that determines the rate of deprotonative C–H cleavage. The reaction was easily scaled up to a gram scale yielding 1.23 g of 34 in 79% yield after recrystallization (Figure 7B). The structure of **34** was unambiguously proved by single crystal X-ray analysis, showing an unprecedented conjugation framework. In sharp contrast to our Fe/Al catalytic system that provided **34** in quantitative yield, the other literature conditions for similar cyclization[38] of oxime or oxime ether employing other metal catalysts such as Co[39], Mn[40], Ru[41], Ir[42], and Rh[43], all failed to react. Only one feasible condition was a rhodium-catalyzed condition elegantly developed by You and co-workers[44], while 20 mol % of rhodium was used with only a moderate yield obtained.

A distinct separation of frontier molecular orbitals was revealed by the calculations. Unlike traditional pentacene structure and derivatives, the integration of imine moiety as electron-accepting units in **ABPhen** (**34**), where the LUMOs locate (Figure 7C), fosters enhanced localization of electron density. Preliminary investigation of the optoelectronic properties of **34** revealed a narrow-band emission at 437 nm with a full width at half maximum (FWHM) of 37 nm and a photoluminescence quantum yield (PLQY) of 21.4% (Figure 7D). This narrowband emission can be ascribed to high symmetry of the rigid conjugation skeleton, resulting in similar molecular geometry between the ground (S_0) and excited (S_1) states that suppress vibronic couplings.[45]

As an interesting candidate for **AAPE**, quinacridone[7-11] has been renowned as a pigment since the last century, its application has been extended to optoelectronic functional materials with applications

found in OLEDs[9], OSCs[10], and OFETs[11]. **AAPE** strategy on quinacridone will result in an unprecedented conjugated skeleton with interesting donor-acceptor structures abbreviated as **DNPA** (Figure 8A). However, C–H activation methods have been rarely successful on quinacridone derivatives. **DNPA** (**35**) was obtained in 80% yield under our optimized Fe/Al conditions. **DNPA** (**35**) is luminescent in the solution and solid state. It exhibited an exceedingly sharp emission at a wavelength of 577 nm, with a very narrow FWHM of 25 nm and a high PLQY value of 87.3% in toluene (Figure 8B). A small Stokes shift of 19 nm in chloroform reveals a weak geometrical distortion between the ground and the excited states. The sharp emission and small Stokes shift can be attributed to the enhanced local transition between the amine donor and imine acceptor, as well as to characteristics inherent to the rigid and symmetrical molecular structures[45].

Theoretical calculation indicates the frontier molecular orbitals are fully delocalized across the fused skeleton, where HOMO and LUMO are largely overlapped (Figure 8C). The time-dependent density functional theory (TD-DFT) analysis revealed that the transition of electrons from the ground state (S_0) to the first excited state (S_1) primarily involves a HOMO to LUMO transfer. This transition is characterized by a notably high oscillator strength (*f*) of 0.5384 and a transition energy of 2.39 eV. The significant value of *f* contributes to an increased fluorescence emission during the S_1 to S_0 transition, resulting in a high PLQY. The current design of donor-acceptor-based emissive materials embeds three coordinated boron atoms as electron-accepting units[46]. The **AAPE** strategy to incorporate imine moiety as electron-accepting units can afford structure of enhanced stability toward moisture and nucleophiles to serve as a platform for the exploration of new types of emissive materials. Notably, a class of **DNPAs** can be easily obtained in good yields by simply diluting with toluene and reprecipitating in methanol after the reaction (see supplementary information), accommodating various alkynes and N-alkyl substituents. This straightforward method provides a convenient route for further synthetic derivatization on **DNPA** core and for convenience in material optimization**.**

In summary, we have developed an iron-catalyzed aza-annulative π-extension strategy with alkynes through direct C–H activation. The strategy catalyzed by an iron/trisphosphine catalyst integrates the use of oxime ether as both an auxiliary for C−H activation and an internal oxidant serving as the nitrogen source, and an isobutyl aluminum catecholate reagent as a base. This efficacious **AAPE** approach is compatible with a broad scope of oxime ethers seamlessly derived from readily available conjugated carbonyl compounds with a variety of alkynes. The expeditious synthesis of π-extended aza-arenes facilitates discoveries in the realm of electronic materials with distinguished electronic and optical properties, as evidenced by the synthesized **Heli-BCIQ** as a prospective CPL material, as well as **ABPhen** and **DNPA** derivatives which showed remarkable emissive properties with narrow emission bands. These findings add new repertoires to our ongoing efforts using iron-catalysis to explore conjugated materials, opening avenues for future development in both materials science and iron-catalyzed C–H activation methodology.

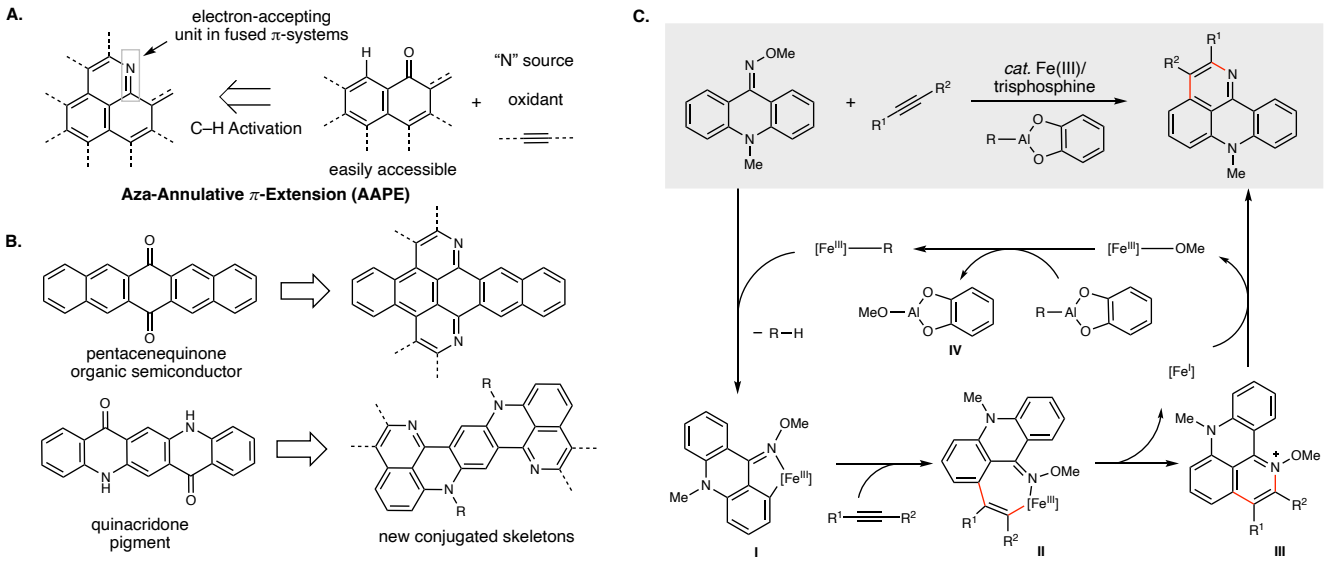

Fig.1| Aza-annulative π-extension (AAPE) with alkynes using iron catalysis. (**A**) The strategy of **AAPE** on easily accessible conjugated ketones via C−H activation. (**B**) **AAPE** as expedient strategy for developing new conjugated skeletons from classical materials, *e.g.* 6,13-pentacenequinone and quinacridone. (**C**) Mechanistic

scenario of iron/TP-catalyzed **AAPE** reaction using an alkyl aluminum reagent as a base and oxime ether as an internal oxidative auxiliary

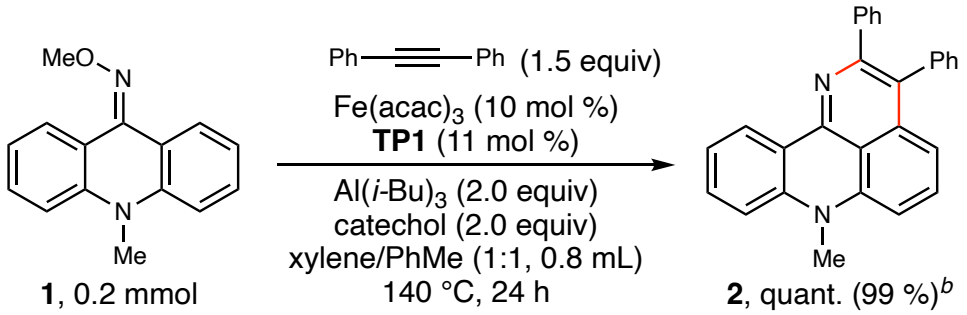

entry	variation from standard condition	yield (%)[a]
1	*w/o* $Fe(acac)_3$	0
2	*w/o* benzofuryl-TP (**TP1**)	25
3	*w/o* catechol	trace
4	*w/o* $Al(i\text{-}Bu)_3$	0
5	$Fe(acac)_3$ (5 mol %) + **TP1** (6 mol %)	90
6	$Fe(acac)_3$ (1 mol %) + **TP1** (2 mol %)	23
7	120 °C instead of 140 °C	91
8	THF instead of xylene	quant.
9	$AlMe_3$ instead of $Al(i\text{-}Bu)_3$	87
10	catechol (2.5 equiv)	18
11	catechol (1.5 equiv)	quant.
12	$Al(i\text{-}Bu)_3$ (1.5 equiv) + catechol (1.0 equiv)	quant.

Fig.2| Investigation of key reaction parameters. [a]Yields were determined with ^{1}H-NMR using 1,3,5-trimethoxybenzene as an internal standard**.** [b]Yield of isolated product.

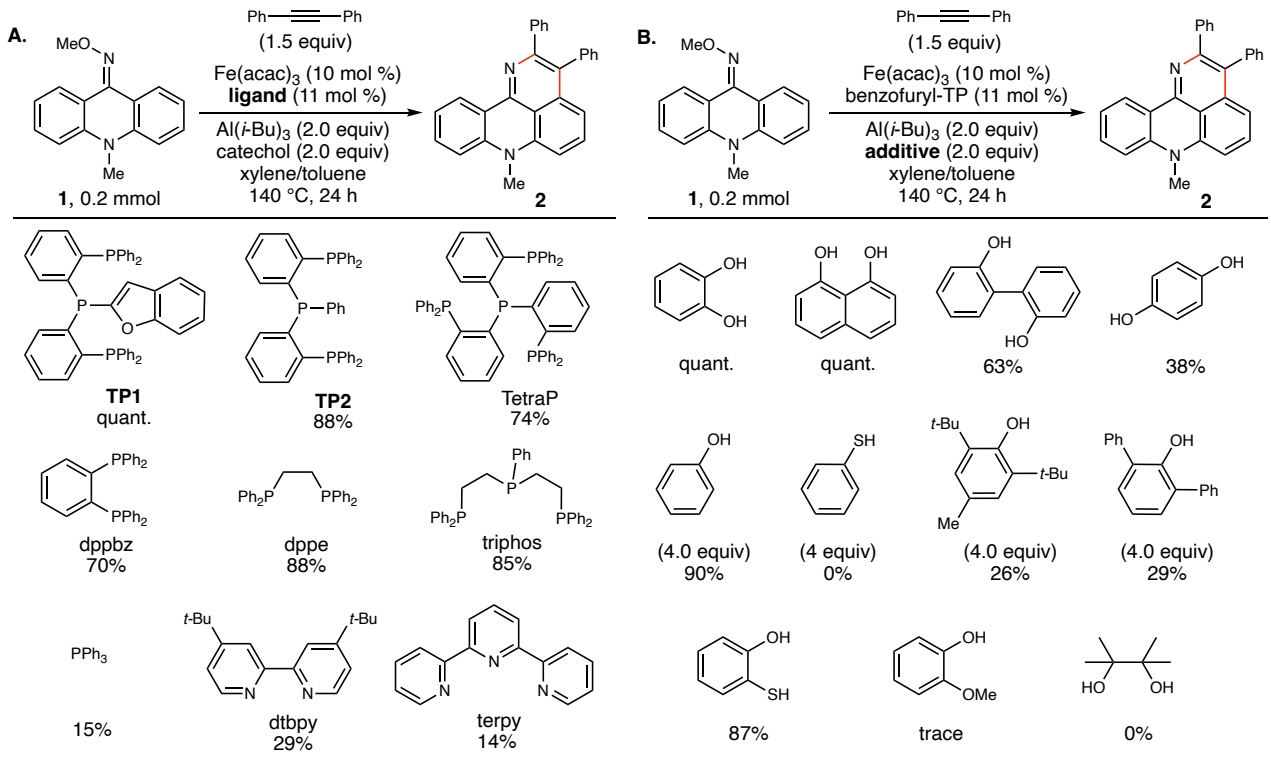

Fig.3| Effects of ligands (A) and phenol additives (B). Yields were determined by ^{1}H NMR using 1,3,5-trimethoxybenzene as an internal standard**.**

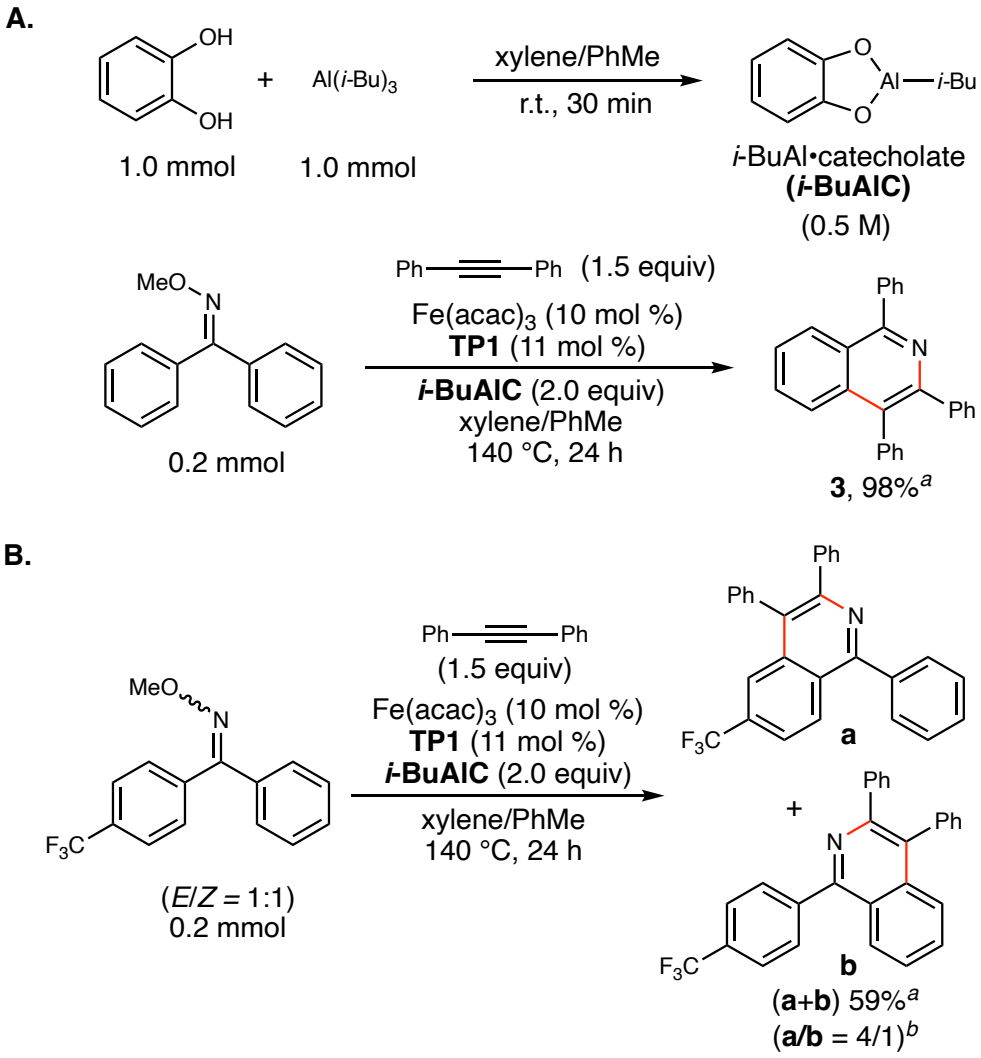

Fig.4| Mechanistic Investigation. (**A**) reaction by using preformed *i*-**BuAlC** reagent. (**B**) Reaction using unsymmetrical oxime ether with Z/E = 1:1. [a]Yields were determined with ^{1}H NMR using 1,3,5-trimethoxybenzene as an internal standard. [b]The ratio was determined by ^{1}H-NMR of the crude mixture.

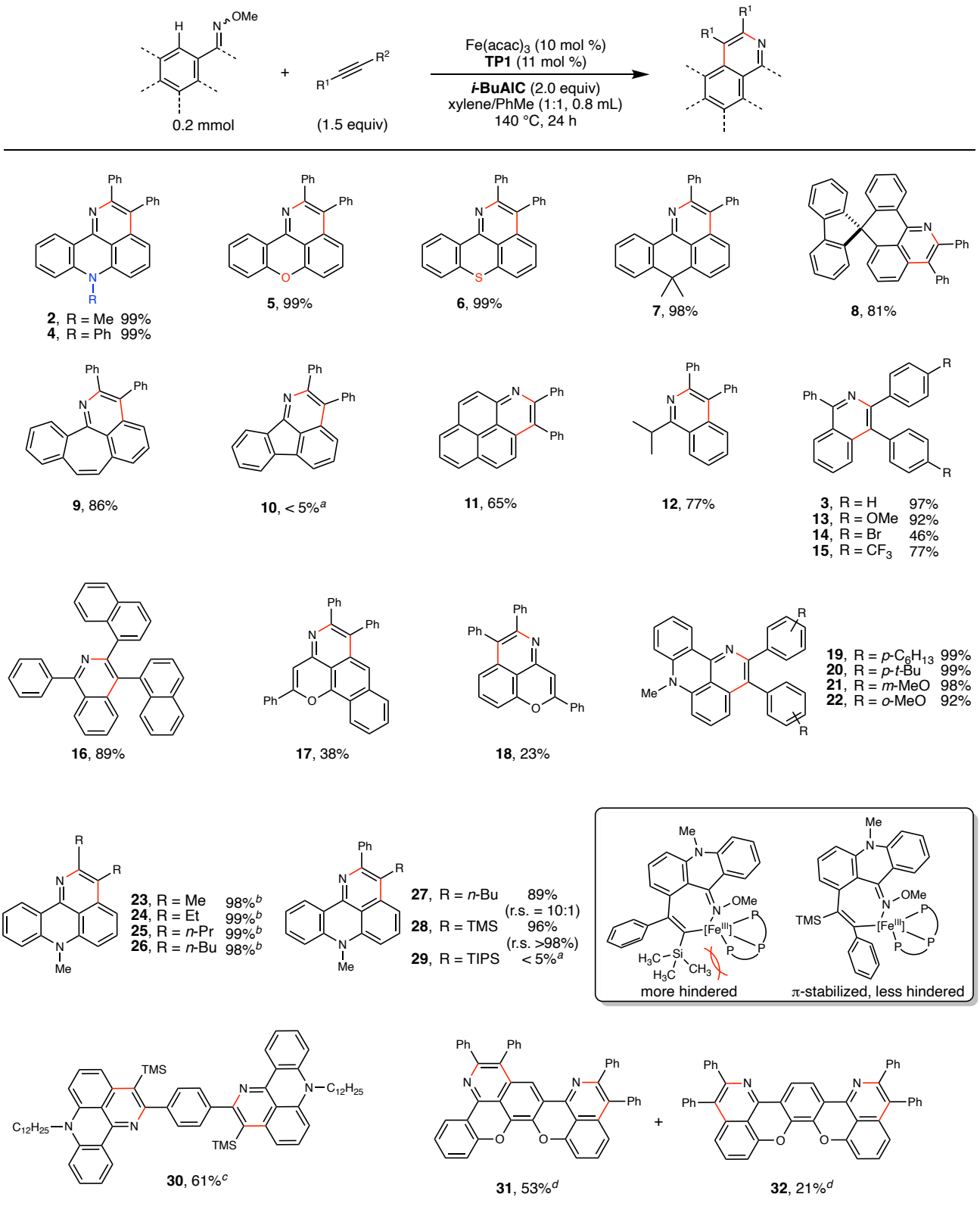

Fig.5| Representative examples of Iron-catalyzed AAPE. [a]Yields were determined by ^{1}H NMR using 1,3,5-trimethoxybenzene as an internal standard. [b]Alkyne used in 2.0 equiv. [c]alkyne (0.10 mmol, 1.0 equiv), oxime (0.22 mmol), $Fe(acac)_3$ (22 mol %), **TP1** (24 mol %), and ***i*-BuAlC** (4.4 equiv). [d]oxime (0.10 mmol, 1.0 equiv), alkyne (0.30 mmol), $Fe(acac)_3$ (20 mol %), **TP1** (22 mol %), and ***i*-BuAlC** (4.0 equiv).

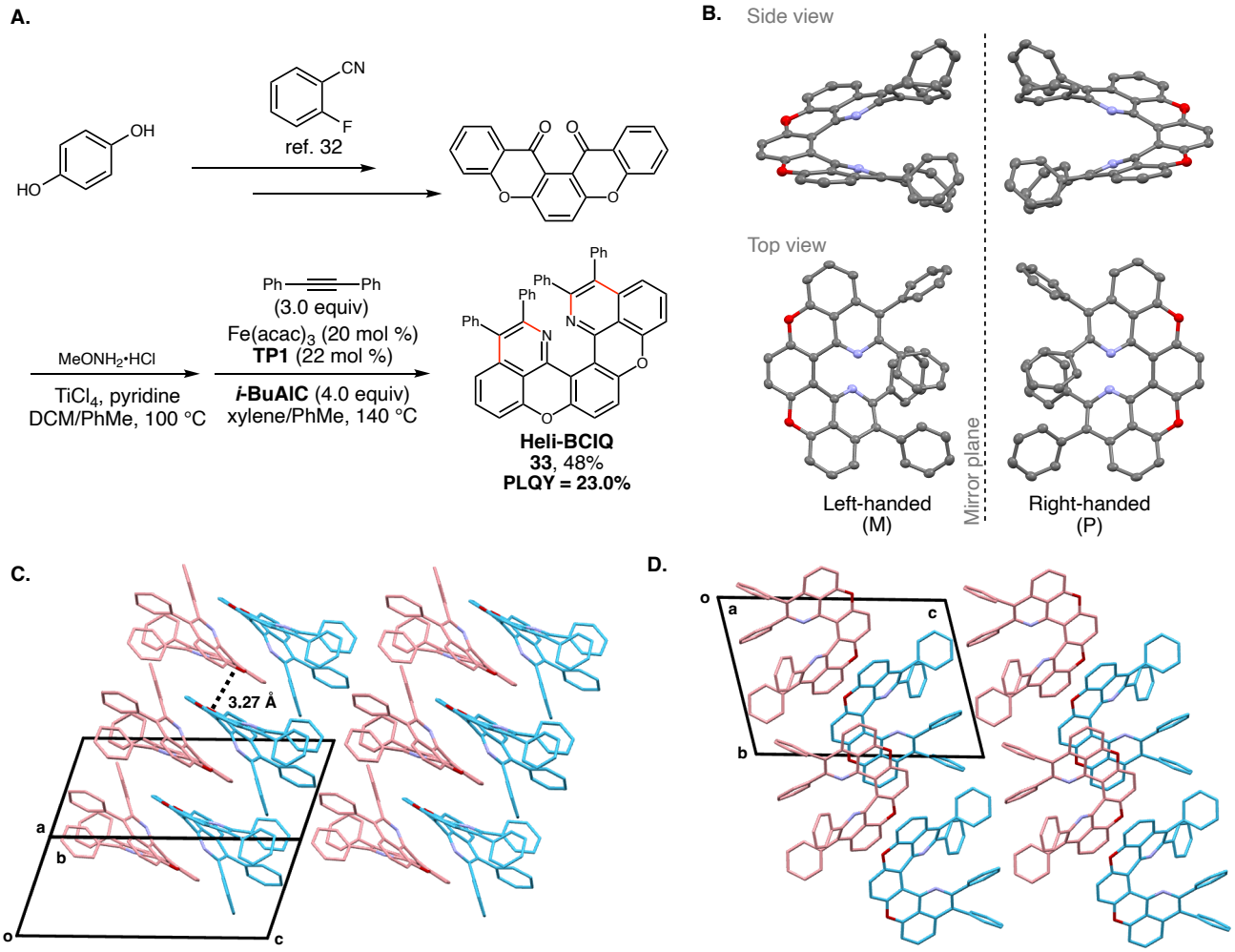

Fig.6| Double AAPE for access to helical-bischromenoisoquinoline (Heli-BCIQ, 33). (**A**) Synthesis of **Heli-BCIQ**. (**B**) Single crystal X-ray structures of each enantiomer of compound **33**. Hydrogen atoms are omitted for clarity. The packing structure of **Heli-BCIQ** along [110] direction (**C**) and along [1-10] (**D**).

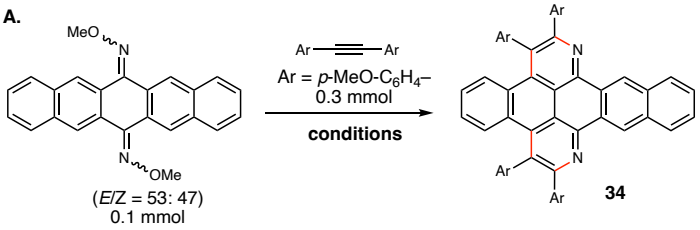

entry	conditions	yield[a]
1	$Fe(acac)_3$ (20 mol %), **TP1** (22 mol %), ***i*-BuAlC** (4.0 equiv), xylene/PhMe, 140 °C, 24 h	99% (r.s. > 99/1)
2	$CoCp^*(CO)I_2$ (10 mol %), KOAc (10 mol %) TFE, 100°C, 24 h	trace
3	$[MnBr(CO)_5]$ (10 mol %), 1,4-dioxane, 105 °C, 12 h	n.d.
4	$[RuCl_2(p\text{-cymene})]_2$ (10 mol %), KPF_6 (60 mol %), MeOH, 60°C, 24 h	n.d.
5	$[Cp^*IrCl_2]_2$ (5 mol %), PivOH (60 mol %) MeOH, 60 °C, 24 h	n.d.
6	$Rh(PPh_3)_3Cl$ (6 mol %), PhMe, 130 °C, 24 h	n.d.
7	$[RhCp^*Cl_2]_2$ (10 mol %), $AgSbF_6$ (40 mol %), THF, 120 °C, 24 h	45% (r.s. > 99/1)

Fig.7| Highly Regioselective double AAPE on pentacene. (**A**) Cyclization of pentacenequinone-derived oxime ether under various reported conditions using other transition metal catalysts. (**B**) Top: isolated yield (gram scale after recrystallization) and single crystal X-ray structure of compound **34**. Hydrogen atoms are omitted for clarity. Bottom: the image of chloroform solutions of **34** under 365 nm UV light irradiation (left), with images of the solids under ambient light (centre) and under 365 nm UV light irradiation (right). (**C**) Frontier molecular orbitals of compound **34** calculated at the B3LYP/6-31+g(d,p) level of theory. (**D**) Absorption and fluorescence spectra of **34** in $CHCl_3$ solution (1.0×10^{-5} M).

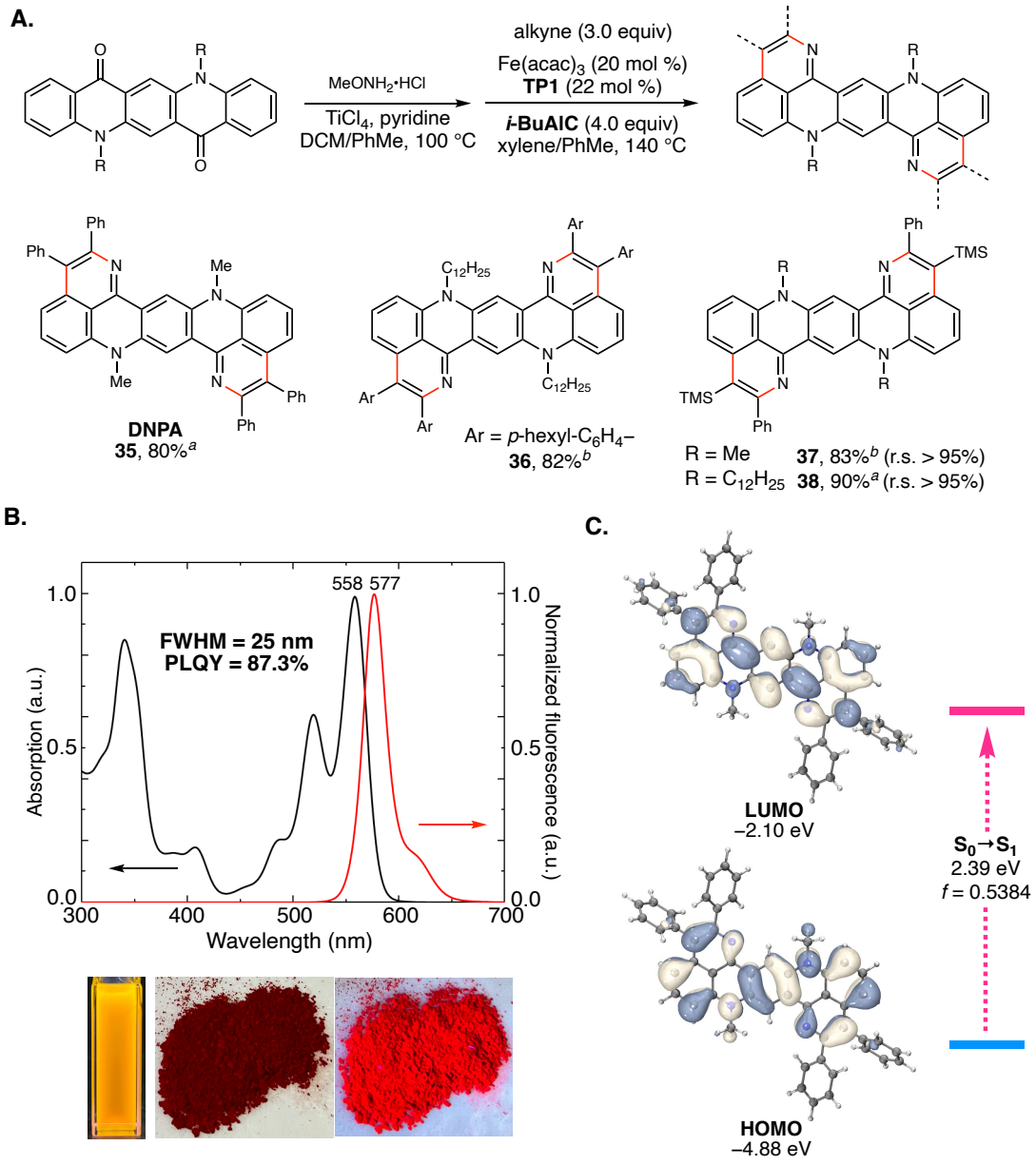

Fig.8| Discovery of new narrow-band emitters (DNPAs) by regioselective AAPE on quinacridone. (**A**) **AAPE** on quinacridone and **DNPAs**. (**B**) Top: absorption and fluorescence spectra of **35** in $CHCl_3$ solution (1.0×10^{-5} M). Bottom: the image of chloroform solutions of **35** under 365 nm UV light irradiation (left), with images of the solids under ambient light (centre) and 365 nm UV light irradiation (right). (**C**) Frontier molecular orbitals of **35** and the corresponding orbital and transition energy levels, along with the *f* values, were calculated at the B3LYP/6-31+g(d,p) level of theory. [a]oxime (0.20 mmol), alkyne (0.60 mmol), $Fe(acac)_3$ (20 mol %), **TP1** (22 mol %), and ***i*-BuAlC** (4.0 equiv). [b]oxime (0.10 mmol), alkyne (0.30 mmol), $Fe(acac)_3$ (20 mol %), **TP1** (22 mol %), and ***i*-BuAlC** (4.0 equiv).

Methods:

General.

All air or moisture-sensitive reactions were performed in a dry reaction vessel under argon atmosphere. Air or moisture-sensitive liquids and solutions were transferred with syringe or Teflon cannula. The water content of solvents was confirmed to be less than 30 ppm by Karl-Fischer titration performed with MKC-210 (Kyoto Electronics Manufacturing Co., Ltd.). Analytical thin-layer chromatography (TLC) was performed with a glass plate coated with 0.25mm 230-400 mesh silica gel containing a fluorescent indicator. Organic solutions were evacuated with a diaphragm pump through a rotary evaporator. Flash column chromatography was performed as described using either Kanto Chemical silica gel 60N as described by Still *et al*.[47]

High-resolution mass spectra (HRMS) were taken with LCMS-IT-TOF (Shimadzu Co.) using reserpine (MW 608.2734) as an internal standard. Nuclear magnetic resonance (NMR) spectra were taken with ECZ-500 (JEOL, Ltd.) at room temperature unless otherwise noted and reported in parts per million (ppm). ^{1}H NMR spectra were internally referenced to tetramethylsilane (0.00 ppm), $CHCl_3$ (7.26 ppm), $CHDCl_2$ (5.32 ppm), C_2HDCl_4 (5.97 ppm), or $(CHD_2)(CD_3)SO$ (2.50 ppm). ^{13}C NMR spectra were internally referenced to tetramethylsilane (0.0 ppm), $CDCl_3$ (77.0 ppm), CD_2Cl_2 (53.8 ppm), $C_2D_2Cl_4$ (73.8 ppm), or $(CD_3)_2SO$ (39.5 ppm). ^{19}F NMR spectra were internally referenced to C_6H_5F (– 113.2 ppm).

Materials.

Unless otherwise noted, reagents were purchased from Tokyo Chemical Industry Co., Ltd., Sigma-Aldrich Co., LCC, FUJIFILM Wako Pure Chemical Co., and other commercial suppliers and were

used as received. Anhydrous tetrahydrofuran, toluene, and dichloromethane were purchased from KANTO Chemical Co., Inc. and purified prior to use by a solvent purification system (GlassContour) equipped with columns of activated alumina and supported copper catalyst. $Fe(acac)_3$ (99.9% trace metal basis) was purchased from Sigma-Aldrich Co., LCC, and used as received. Xylene was purchased from FUJIFILM Wako Pure Chemical Co., degassed by Freeze-Pump-Thaw cycling for three times, dried with molecular sieves 4Å, and kept in a storage flask.

A general procedure for cyclization of *O*-methyl oxime with alkynes

In an oven-dried Schlenk tube, an oxime ether (0.20 mmol), an alkyne (0.30 mmol, or 0.40 mmol for dialkyl acetylene), catechol (44 mg, 0.40 mmol), TP1 (15 mg, 0.022 mmol), $Fe(acac)_3$ (7.0 mg, 0.020 mmol), and xylene (0.40 mL) were combined. Subsequently, a solution of Al(*i*-Bu)$_3$ in toluene (1.0 mol/L, 0.40 mL, 0.40 mmol) was added by rinsing the inner walls of the Schlenk tube at room temperature. The reaction mixture was stirred at room temperature for 5 minutes to allow generation of *i*-BuAl·catecholate in-situ and then at 140 ℃ for 24 hours. After completion, the reaction mixture was cooled to room temperature, diluted with dichloromethane (2 mL) or toluene (2 mL), and carefully quenched with methanol (0.1 mL). Then, solvents were removed under reduced pressure. The crude product was directly purified through silica gel chromatography or reprecipitation.

Data availability

All of the data supporting the findings of this study, including experimental procedures and compound characterization, are available within the paper and its Supplementary Information, or

from the authors upon reasonable request. CCDC 2323874 (**O16**), CCDC 2323875 (**33**), and CCDC 2323876 (**34**) contain the supplementary crystallographic data for this paper. The data can be obtained free of charge from The Cambridge Crystallographic Data Centre via www.ccdc.cam.ac.uk/structures.

Author Contributions

R.S. and E.N. conceived the idea and guided the research project. Y.Z. conducted the experiments to study the reaction parameters, scope, material properties, and prepared the SI. S.F. conducted the single crystal X-ray analysis. The manuscript was written through the contributions of all authors.

Competing interests

The authors declare the following competing financial interest(s): E.N., R.S., and Y.Z are inventors on Japanese patent application No. 2023-185412 submitted by the University of Tokyo, which covers synthetic methods and compound structures described in this manuscript.

Acknowledgments

We thank Mitsubishi Chemical Corporation for partial financial support. This research is supported by MEXT KAKENHI grant number 19H05459 (to E.N.), JSPS KAKENHI grant number 19K15555 (to R.S.), and JST SPRING, Grant Number JPMJSP2108 (to Y.Z.).

References

1. Enthaler, S., Junge, K. & Beller, M. Sustainable metal catalysis with iron: From rust to a rising star? *Angew. Chem., Int. Ed.* **47**, 3317-3321 (2008).

2. Stepek, I. A. & Itami, K. Recent Advances in C-H Activation for the Synthesis of π-Extended Materials. *ACS Mater. Lett.* **2**, 951-974 (2020).

3. Patel, D. G. *et al.* It takes more than an imine: the role of the central atom on the electron-accepting ability of benzotriazole and benzothiadiazole oligomers. *J. Am. Chem. Soc.* **134**, 2599-2612 (2012).

4. Bhattacharjee, M. N., Chaudhuri, M. K., Dasgupta, H. S., Roy, N. & Khathing, D. T. Pyridinium fluorochromate; A new and efficient oxidant for organic substrates. *Synthesis* **1982**, 588-590 (1982).

5. Vets, N., Smet, M. & Dehaen, W. Synthesis and thermolysis of a Diels–Alder adduct of pentacene and thiophosgene. *Tetrahedron Lett.* **45**, 7287-7289 (2004).

6. Liang, Z. *et al.* N-Type Organic Semiconductors Based on π-Deficient Pentacenequinones: Synthesis, Electronic Structures, Molecular Packing, and Thin Film Transistors. *Chem. Mater.* **22**, 6438-6443 (2010).

7. Labana, S. & Labana, L. Quinacridones. *Chem. Rev.* **67**, 1-18 (1967).

8. Wang, C., Zhang, Z. & Wang, Y. Quinacridone-based π-conjugated electronic materials. *J. Mater. Chem. C* **4**, 9918-9936 (2016).

9. Shi, J. & Tang, C. W. Doped organic electroluminescent devices with improved stability. *Appl. Phys. Lett.* **70**, 1665-1667 (1997).

10. Chen, J. J.-A. *et al.* Quinacridone-based molecular donors for solution processed bulk-heterojunction organic solar cells. *ACS Appl. Mater. Interfaces* **2**, 2679-2686 (2010).

11. Daniel Głowacki, E. *et al.* Intermolecular hydrogen-bonded organic semiconductors—Quinacridone versus pentacene. *Appl. Phys. Lett.* **101** (2012).

12. Shang, R., Ilies, L. & Nakamura, E. Iron-catalyzed C–H bond activation. *Chem. Rev.* **117**, 9086-9139 (2017).

13. Huang, H., Ji, X., Wu, W. & Jiang, H. Transition metal-catalyzed C–H functionalization of N-oxyenamine internal oxidants. *Chem. Soc. Rev.* **44**, 1155-1171 (2015).

14. Borissov, A. *et al.* Recent advances in heterocyclic nanographenes and other polycyclic heteroaromatic compounds. *Chem. Rev.* **122**, 565-788 (2021).

15. Bunz, U. H. The larger linear N-heteroacenes. *Acc. Chem. Res.* **48**, 1676-1686 (2015).

16. Anthony, J. E. Functionalized acenes and heteroacenes for organic electronics. *Chem. Rev.* **106**, 5028-5048 (2006).

17. Shang, R., Ilies, L. & Nakamura, E. Iron-catalyzed directed C (sp2)–H and C (sp3)–H functionalization with trimethylaluminum. *J. Am. Chem. Soc.* **137**, 7660-7663 (2015).

18. Shang, R., Ilies, L. & Nakamura, E. Iron-catalyzed ortho C–H methylation of aromatics bearing a simple carbonyl group with methylaluminum and tridentate phosphine ligand. *J. Am. Chem. Soc.* **138**, 10132-10135 (2016).

19. Doba, T., Ilies, L., Sato, W., Shang, R. & Nakamura, E. Iron-catalysed regioselective thienyl C–H/C–H coupling. *Nat. Catal.* **4**, 631-638 (2021).

20. Doba, T., Shang, R. & Nakamura, E. Iron-Catalyzed C–H Activation for Heterocoupling and Copolymerization of Thiophenes with Enamines. *J. Am. Chem. Soc.* **144**, 21692-21701 (2022).

21. Doba, T., Fukuma, S., Shang, R. & Nakamura, E. Versatile Synthesis of Trisphosphines Bearing Phenylene and Vinylene Backbones Useful for Metal Catalysis and Materials Applications. *Synthesis* **55**, 1690-1699 (2023).

22. Jana, R., Pathak, T. P. & Sigman, M. S. Advances in transition metal (Pd, Ni, Fe)-catalyzed cross-coupling reactions using alkyl-organometallics as reaction partners. *Chem. Rev.* **111**, 1417-1492 (2011).

23. Boone, S. R. *et al.* Magnetic exchange interactions in semiquinone complexes of iron. Structural and magnetic properties of tris (3, 5-di-tert-butylsemiquinonato) iron (III) and tetrakis (3, 5-di-tert-butylsemiquinonato) tetrakis (3, 5-di-tert-butylcatecholato) tetrairon (III). *J. Am. Chem. Soc.* **111**, 2292-2299 (1989).

24. DeMuth, J. C. *et al.* Experimental and computational studies of the mechanism of iron-catalysed C–H activation/functionalisation with allyl electrophiles. *Chem. Sci.* **12**, 9398-9407 (2021).

25. Hatakeyama, T. *et al.* Iron-Catalyzed Suzuki−Miyaura Coupling of Alkyl Halides. *J. Am. Chem. Soc.* **132**, 10674-10676 (2010).

26. Saito, S. & Yamamoto, H. Designer Lewis acid catalysts—bulky aluminium reagents for selective organic synthesis. *Chem. Commun.*, 1585-1592 (1997).

27. Verma, A. K. & Pratap, R. The biological potential of flavones. *Nat. Prod. Rep.* **27**, 1571-1593 (2010).

28. Badea, M. *et al.* Thermal behavior of some vanadyl complexes with flavone derivatives as potential insulin-mimetic agents. *J. Therm. Anal. Calorim.* **105**, 559-564 (2011).

29. Schönherr, H. & Cernak, T. Profound Methyl Effects in Drug Discovery and a Call for New C−H Methylation Reactions. *Angew. Chem., Int. Ed.* **52**, 12256-12267 (2013).

30. Liu, J., Liu, J., Li, H., Bin, Z. & You, J. Boron-Dipyrromethene-Based Fluorescent Emitters Enable High-Performance Narrowband Red Organic Light-Emitting Diodes. *Angew. Chem., Int. Ed.* **62**, e202306471 (2023).

31. Wilson, S. R. & Jacob, L. A. Iodination of aryltrimethylsilanes. A mild approach to (iodophenyl)alanine. *J. Org. Chem.* **51**, 4833-4836 (1986).

32. Wang, B. *et al.* Synthesis of Di- and Trixanthones that Display High Stability and a Visual Fluorescence Response to Strong Acid. *Chem. – Asian J.* **9**, 3307-3312 (2014).

33. Zhao, W.-L., Li, M., Lu, H.-Y. & Chen, C.-F. Advances in helicene derivatives with circularly polarized luminescence. *Chem. Commun.* **55**, 13793-13803 (2019).

34. Mota, M. L. *et al.* Fast and inexpensive synthesis of pentacene with high yield using 6, 13-pentacenequinone as precursor. *J. Mol. Struct.* **1154**, 511-515 (2018).

35. Roberson, L. B. *et al.* Pentacene Disproportionation during Sublimation for Field-Effect Transistors. *J. Am. Chem. Soc.* **127**, 3069-3075 (2005).

36. Wu, M.-X. *et al.* Functionalization of pentacene: a facile and versatile approach to contorted polycyclic aromatic hydrocarbons. *Angew. Chem., Int. Ed.*, e202309619 (2023).

37. Miao, Q. Ten Years of N-Heteropentacenes as Semiconductors for Organic Thin-Film Transistors. *Adv. Mater.* **26**, 5541-5549 (2014).

38. He, R., Huang, Z.-T., Zheng, Q.-Y. & Wang, C. Isoquinoline skeleton synthesis via chelation-assisted C− H activation. *Tetrahedron Lett.* **55**, 5705-5713 (2014).

39. Muralirajan, K., Kuppusamy, R., Prakash, S. & Cheng, C.-H. Easy Access to 1-Amino and 1-Carbon Substituted Isoquinolines via Cobalt-Catalyzed C−H/N−O Bond Activation. *Adv. Synth. Catal.* **358**, 774-783 (2016).

40. He, R., Huang, Z.-T., Zheng, Q.-Y. & Wang, C. Manganese-Catalyzed Dehydrogenative [4+2] Annulation of N−H Imines and Alkynes by C−H/N−H Activation. *Angew. Chem., Int. Ed.* **53**, 4950-4953 (2014).

41. Kornhaaß, C., Li, J. & Ackermann, L. Cationic Ruthenium Catalysts for Alkyne Annulations with Oximes by C–H/N–O Functionalizations. *J. Org. Chem.* **77**, 9190-9198 (2012).

42. Lin, W., Hu, X.-X., Zhuang, C.-W. & Wang, Y.-Z. Easy access to synthesize isoquinolines from aryl ketoximes and internal alkynes via Iridium (III)-catalyzed CH/NO bond activation. *Tetrahedron* **75**, 3015-3023 (2019).

43. Parthasarathy, K. & Cheng, C.-H. Easy Access to Isoquinolines and Tetrahydroquinolines from Ketoximes and Alkynes via Rhodium-Catalyzed C−H Bond Activation. *J. Org. Chem.* **74**, 9359-9364 (2009).

44. Li, C. *et al.* Direct [4+ 2] Cycloaddition to Isoquinoline-Fused Porphyrins for Near-Infrared Photodynamic Anticancer Agents. *Org. Lett.* **24**, 175-180 (2021).

45. Ha, J. M., Hur, S. H., Pathak, A., Jeong, J.-E. & Woo, H. Y. Recent advances in organic luminescent materials with narrowband emission. *NPG Asia Mater.* **13**, 53 (2021).

46. Hatakeyama, T. *et al.* Ultrapure blue thermally activated delayed fluorescence molecules: efficient HOMO–LUMO separation by the multiple resonance effect. *Adv. Mater.* **28**, 2777-2781 (2016).

47. Still, W. C., Kahn, M. & Mitra, A. Rapid chromatographic technique for preparative separations with moderate resolution. *J. Org. Chem.* **43**, 2923–2925 (1978).